IEEE Access
Multidisciplinary | Rapid Review | Open Access Journal

Received 4 October 2023, accepted 20 October 2023, date of publication 25 October 2023, date of current version 1 November 2023.

Digital Object Identifier 10.1109/ACCESS.2023.3327429

RESEARCH ARTICLE

Propagation Analysis Using Discrete Mixed Fourier Transform-Based Parabolic Equation Method for Long Range Radar Detection Error Correction

JUN HEO[1], (Graduate Student Member, IEEE), JUNMO YANG[1], (Graduate Student Member, IEEE), JONGMANN KIM[2], DONG-YEOP NA[3], (Member, IEEE), AND YONG BAE PARK[1,4], (Senior Member, IEEE)

[1]Department of AI Convergence Network, Ajou University, Suwon 16499, South Korea
[2]Agency for Defense Development, Daejeon 34316, South Korea
[3]Department of Electrical Engineering, Pohang University of Science and Technology, Pohang 37673, South Korea
[4]Department of Electrical and Computer Engineering, Ajou University, Suwon 16499, South Korea

Corresponding author: Yong Bae Park (yong@ajou.ac.kr)

This work was supported by the Agency for Defense Development by the Korean Government under Grant UD210013YD.

ABSTRACT This paper proposes a novel method to predict the radar detection errors in a complex environment by considering slant range and angular error. This method involves analysis of the electromagnetic wave propagation path loss in troposphere using discrete mixed Fourier transform based split–step parabolic equation. For analysis, modeling of the terrain profile using a digital elevation model and estimating the refractive index by interpolating upper–air observations is conducted. The direction of refracted antenna's main beam is predicted using the path loss, and by comparing it with the antenna boresight, the radar errors are computed according to the received timing of the radar echo. To apply the proposed method to real scenarios, the atmospheric environment within the analysis area is modeled using meteorological data collected on a specific day. By applying the proposed method to an arbitrary date and location, the radar errors in a long–range propagation environment where refraction occurs are analyzed.

INDEX TERMS Angular error, parabolic equation method, radar detection, slant range error.

I. INTRODUCTION

The performance of radar systems is heavily influenced by the propagation environment over the detection area. In long–range radar detection, where ranges can span hundreds of kilometers, electromagnetic (EM) waves can undergo several effects such as refraction, reflection, shielding, and diffraction due to complex atmospheric and geographical conditions. These effects can lead to errors in radar detection performances, making it essential to accurately model the propagation in complex domains and predict radar errors.

In the early studies, propagation modeling in the troposphere was developed by Norton [1] and Wait [2], which were applicable only to the smooth spherical Earth. Although an analysis method for a smooth Earth considering the transition from sea to land was proposed [3], [4], these methods were unable to account for irregular terrain in the calculation. Moreover, various numerical methods have been employed to investigate EM wave propagation, including mode theory, geometrical optics (GO), and the parabolic equation (PE) method [5], [6]. However, in long–range environments, several factors need to be considered, such as the curvature of the Earth, irregular terrain, and range–dependent atmospheric conditions. In such complex conditions, the mode theory requires intensive computational load, and GO is challenging to apply to environments where range–dependent factors play a significant role. In contrast, the PE method can handle range–dependent conditions with

The associate editor coordinating the review of this manuscript and approving it for publication was Sandra Costanzo.

relatively less computational burden. Hence, the PE method is suitable for analyzing the EM wave propagation of long–range radar systems.

The PE method initially proposed by Leontovich and Fock [7] in the 1940s for trans–horizon EM wave propagation modeling. The PE method had not been very efficient until the split–step PE (SSPE) algorithm was developed by Hardin and Tappert [8] in 1973. The SSPE method involves numerically discretizing the analysis domain from the antenna source to the end and then advancing the analysis step by step. By using this approach, the SSPE method provides accurate modeling of EM wave propagation over a large area. Since then, it has been widely utilized in various propagation modeling analyses due to its improved efficiency and accuracy [9], [10], [11], [12], [13], [14].

For long–range environments, important factors mentioned above can be considered in analysis using the SSPE method. First, the flat Earth model can be used to consider the curvature of Earth and enhance visibility of results. The concept of modified refractive index is utilized to compensate for changes in refractivity resulting from the flattening of the Earth. Additionally, the mechanism of the SSPE method, which advances and analyzes step by step, can reflect the range–dependent refractivity and irregular terrain profile.

Furthermore, the impedance boundary condition of analysis area is variable in long–range environments, such as sea–land or sea–land–sea regions. To account the inhomogeneous impedance boundary condition, a discrete mixed Fourier transform (DMFT) based SSPE method was introduced [15], [16], [17], [18], [19]. The propagation analysis for sea and land transition can be performed using the DMFT based SSPE method, which considers the impedance at each boundary. By allocating the different permittivity and conductivity for the sea and land boundaries, it is possible to accurately predict the behavior of EM waves as they propagate through these region.

Recently, several studies have been proposed using the PE method to model EM wave propagation in complex environments. For instance, a hybrid method of PE and finite difference time domain method was utilized to predict radar target echo signals in large–scale complex environments [20]. In another study, the PE method was applied to predict propagation in a complex environment with sea surface and forest [21]. In a third study, the PE method was used to analyze path loss in air–to–ground radar applications [22].

To the best of our knowledge, studies about analyzing the radar errors that may occur due to large and complex environments seem to be lacking. In such environments, the propagation of EM waves may differ from the prediction and it causes errors in radar measurements. Therefore, it is essential to analyze radar errors that may occur in such environments.

In this paper, we propose a novel method to predict the radar detection errors for long–range radar. The system is set to S band radar used for target detection. Since the detection of the target proceeds over long distances, a low grazing angle is applied on the sea surface. On this system, the sea surface is sometimes regarded as the same as perfect electric conductor (PEC) [23]. However, when the terrain exists, the grazing angle increases, so impedance boundary condition is required on analysis. Therefore, we use DMFT based SSPE to analyze the propagation of EM waves with impedance boundary condition. The different relative permittivity and conductivity on impedance boundary condition to classify the sea ($\epsilon_r = 80, \sigma = 5$ S/m) and land ($\epsilon_r = 2, \sigma = 0.01$ S/m) are used respectively [5]. Using DMFT based SSPE results, we predict the refracted antenna's main beam direction, and the distance traveled on that path and boresight is calculated using the radar echo signal timing. Comparing the results, the slant range and angular error are analyzed over the analysis area.

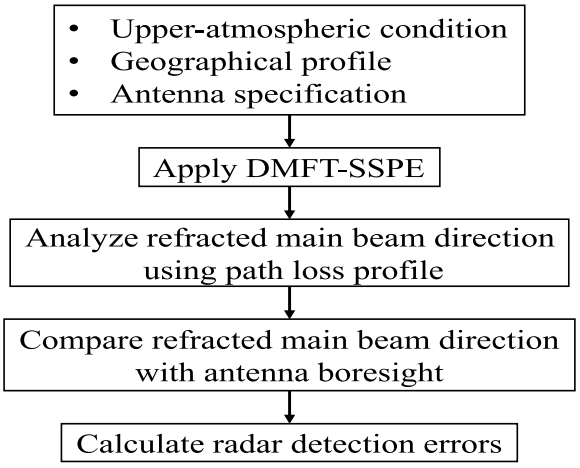

FIGURE 1. Schematic of the proposed method.

This paper is organized as follows: Section II provides an overview of the parameters utilized in the analysis of EM wave propagation, along with the modeling techniques employed. Additionally, a concise summary of the DMFT–SSPE method is presented, highlighting its relevance to the study. Section III introduces the method employed for predicting the refracted antenna's main beam direction. This prediction is based on an analysis of the path loss outcomes, allowing for insightful observations across diverse atmospheric conditions. Section IV provides a detailed analysis of radar errors, specifically by examining the errors associated with slant range and elevation angle. This analysis takes into consideration an atmospheric environment model that has been constructed using measurement data. The schematic of the method proposed in this paper is shown in Fig 1.

II. PROPAGATION ENVIRONMENT MODELING AND DMFT–BASED SSPE METHOD

A. GEOGRAPHICAL AND ATMOSPHERIC ENVIRONMENTS

Accurate modeling of geographical profile and atmospheric environments is crucial for analyzing the propagation of EM waves in a long–range environment, as illustrated in Fig. 2. A geographical profile can be obtained by

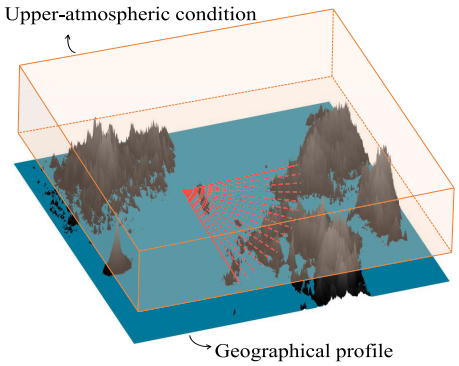

FIGURE 2. Geographical profile and atmospheric conditions surrounding radar position and analysis area. The location of the radar is represented by a red inverted triangle, which is arbitrarily determined. The analysis area is set to 90° counterclockwise from the south.

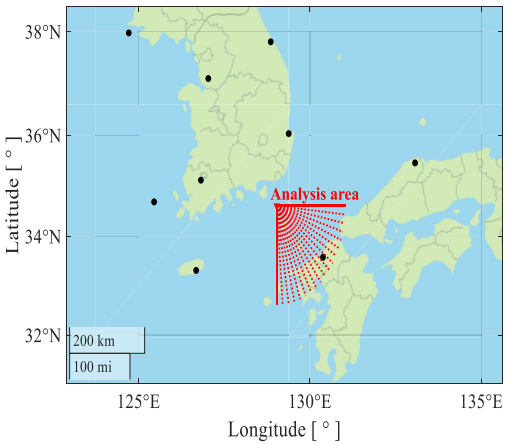

FIGURE 3. Details of the surroundings of the radar and location of the meteorological observation stations (black dots). Measurement data from the stations can be used as a known point in interpolating the refractivity.

calculating the elevation of the terrain corresponding to each distance in a DEM. The atmospheric environment can be modeled by calculating the refractivity based on various meteorological data [24]. However, obtaining data for the entire analysis domain can be a difficult task. This is why regular meteorological measurements conducted by some stations using rawinsondes can be useful. By obtaining data on temperature, air pressure, and water vapor pressure by altitude, two dimensional interpolation can be performed to model the atmospheric environment for the analysis area. For the analysis, it is assumed that the radar is located in the sea near Pohang in South Korea. Details of the surroundings of this location and meteorological observations stations are illustrated in Fig. 3. By utilizing the atmospheric data obtained from these sites, it is possible to calculate the refractivity N and refractive index n [24]

$$\begin{aligned} N &= (n-1)\times 10^6 \\ &= 77.6\frac{P}{T} + 3.73\times 10^5 \frac{e}{T^2} \end{aligned} \tag{1}$$

where P is the pressure in mbar, T is the absolute temperature in $^\circ K$, and e is the partial pressure of water vapor in mbar.

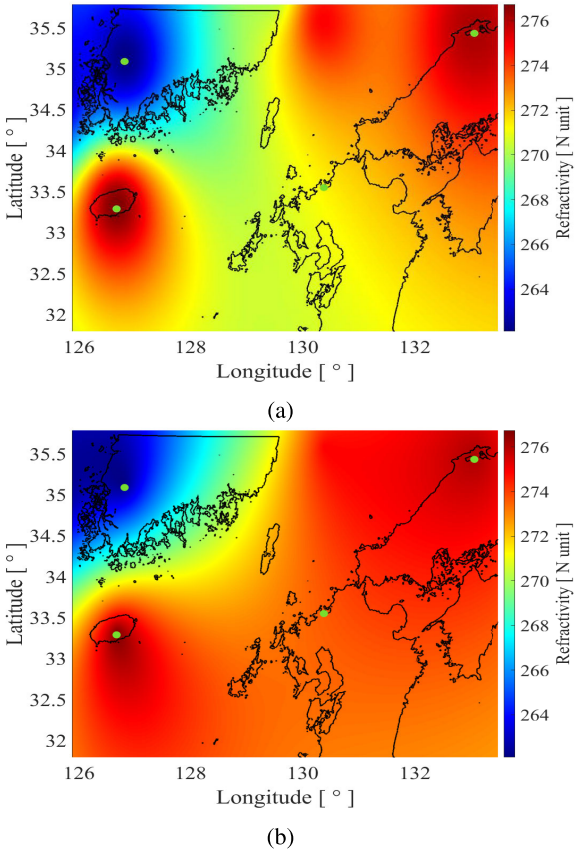

FIGURE 4. 2D interpolation of refractivity N on January 12th, 2023. The values at an altitude of 1 km is shown as an example, and locations of the stations are indicated by green dots. (a) IDW interpolation. (b) kriging interpolation.

Refraction can cause EM waves to bend up or down along Earth's surface, allowing them to propagate beyond the radar horizon. To accurately account for this effect, two methods are commonly used. The first involves using N, which assumes an effective Earth radius. The second method utilizes the modified refractivity M [24], which accounts for the curvature of Earth

$$M = (n + x/a_e - 1)\times 10^6 \tag{2}$$

where x means the height in kilometers, a_e is radius of Earth, that is 6,378 km. The modified refractivity M can provide more accurate results in long–range analysis because it considers the curvature of Earth. Depending on the vertical gradient of M, the refraction can be classified into four types, such as sub, super, standard and duct. Accurately modeling the atmospheric environment is crucial for predicting the propagation of EM waves in long–range environments. However, collecting atmospheric data at all points in the analysis area is practically impossible. Hence, it is practical to interpolate data using known points, illustrated in Fig. 3. Two straightforward methods for this are inverse distance weighting (IDW) and the kriging [25], [26]. IDW estimates values at unknown points based on their distance from known points. Kriging, on the other hand, considers both distance

and correlation between neighboring known points. While kriging can be more computationally demanding than IDW, it yields superior results when dealing with intricate spatial data patterns.

However, due to the sparse distribution of known points, they are less correlated with each other. Therefore, determining the superiority of kriging over IDW in terms of accuracy is difficult. This trend is evident in Fig. 4, where (a) and (b) show the distribution of N at an altitude of 1 km calculated by interpolating weather data at known points using IDW and kriging respectively. While there are slight differences in the outcomes of the two horizontal interpolations, the overall trends remain largely consistent. As a result, the results of propagation analysis exhibit minimal variation.

B. THE METHOD OF THE EM WAVE PROPAGATION ANALYSIS: DMFT–BASED SSPE

The PE method is a strategy for solving problems by simplifying the 3D scenario between the transmitter and the receiver into a 2D projection, which allows for easier analysis and computation. In an environment where only range and height are considered, the field component satisfies the 2D Helmholtz equation [5]

$$\frac{\partial^2 U}{\partial z^2} + \frac{\partial^2 U}{\partial x^2} + k_0^2 n^2 U = 0 \tag{3}$$

where $U(z, x)$ represents either electric or magnetic field for horizontal and vertical polarization, k_0 is the free space wavenumber, n is the refractive index, z and x stand for the range and height, respectively. When the propagation is predominantly in the +z direction, the field component $U(z, x)$ can be paraxially approximated by

$$U(z, x) = e^{ik_0 z} u(z, x) \tag{4}$$

where $e^{ik_0 z}$ represents a rapidly varying phase term and $u(z, x)$ means the reduced field strength function.

In scenarios where the EM wave propagates in the paraxial direction along a smooth sea surface, the angle of incidence remains exceedingly small. Consequently, the reflection coefficient at sea surface approximates -1 [23]. In this case, the boundary condition can be treated like a PEC. However, the introduction of terrain features, such as islands, leads to an elevation in the incidence angle of the EM wave. Consequently, this situation demands the inclusion of an impedance boundary condition into the analysis. For such situations, the DMFT based SSPE can be applied as follows [18]

$$U(z, 0) = A \sum_{m=0}^{N} r^m u(z, m\Delta x) \tag{5}$$

$$U(z, l\Delta k_x) = \sum_{m=0}^{N} \left[\alpha(z) sin\left(\frac{\pi lm}{N}\right) - \frac{1}{\Delta x} sin\left(\frac{\pi l}{N}\right) cos\left(\frac{\pi lm}{N}\right) \right] \times u(z, m\Delta x) \tag{6}$$

$$U(z, N\Delta k_x) = A \sum_{m=0}^{N} (-r)^{N-m} u(z, m\Delta x) \tag{7}$$

where $A = 2(1 - r^2)/\left[(1 + r^2)(1 - r^{2N})\right]$, $l = 1, \cdots, N - 1$, Δk_x is the spacing in transform space correspond to $\Delta k_x \Delta x = \pi/N$, and r is the roots of $r^2 + 2\alpha\Delta x - 1 = 0$ with smaller magnitude. The constant $\alpha(z)$ can be introduced with $\alpha(z) = ik_0\sqrt{\gamma - 1}/\gamma$ and $\alpha(z) = ik_0\sqrt{\gamma - 1}$ ($\gamma = \epsilon_r(z) + i60\sigma(z)\lambda$) for vertical and horizontal polarizations, respectively [18]. Additionally, a weight of 0.5 is assigned to both the initial and last terms of summations. Then, U at the advanced range $z + \Delta z$ is calculated using

$$U(z + \Delta z, 0) = exp\left(\frac{i\Delta z}{2k_0}\left(\frac{log(r)}{\Delta x}\right)^2\right) U(z, 0) \tag{8}$$

$$U(z + \Delta z, l\Delta k_x) = exp\left(i\Delta z\left(\sqrt{k_0^2 - (l\Delta k_x)^2} - k_0\right)\right) \times U(z, l\Delta k_x) \tag{9}$$

$$U(z + \Delta z, N\Delta k_x) = exp\left(\frac{i\Delta z}{2k_0}\left(\frac{log(-r)}{\Delta x}\right)^2\right) \times U(z, N\Delta k_x) \tag{10}$$

where Δz is typically set larger than the wavelength in the process of discretizing the domain in the SSPE method. Finally, the field strength at advanced range can be obtained using inverse DMFT.

$$\begin{aligned} u(z + \Delta z, m\Delta x) = {} & U(z + \Delta z, 0) r^m \\ & + U(z + \Delta z, N\Delta k_x)(-r)^{N-m} \\ & + \frac{2}{N} \sum_{l=0}^{N} U(z + \Delta z, l\Delta k_x) \times B(l) \\ B(l) = {} & \frac{\alpha(z) sin\left(\frac{\pi lm}{N}\right) - \frac{1}{\Delta x} sin\left(\frac{\pi l}{N}\right) cos\left(\frac{\pi lm}{N}\right)}{\alpha^2(z) + \frac{1}{\Delta x^2} sin^2\left(\frac{\pi l}{N}\right)} \end{aligned} \tag{11}$$

The calculation of SSPE can then be performed by multiplying the derived $u(z, x)$ with an exponential term that corresponds to the propagation.

III. PREDICTION OF THE REFRACTED DIRECTION OF ANTENNA'S MAIN BEAM

A. ANTENNA MODELING AND BORESIGHT CONSIDERING THE EARTH FLATTENING

The propagation analysis using SSPE method involves calculating the vertical field profile in each range step based on the profile from the previous step. To start this process, an initial value is needed. One way to obtain this is by modeling the aperture field with the transmission antenna pattern at an initial range point. By utilizing an appropriate antenna pattern and the near field/far field relationship, it is possible to calculate the initial reduced vertical field profile as [5]

$$u(0, x) = \int_{-\frac{1}{\lambda}}^{+\frac{1}{\lambda}} \frac{B(\theta(p))}{\sqrt{cos(\theta(p))}} e^{2i\pi px} dp \tag{12}$$

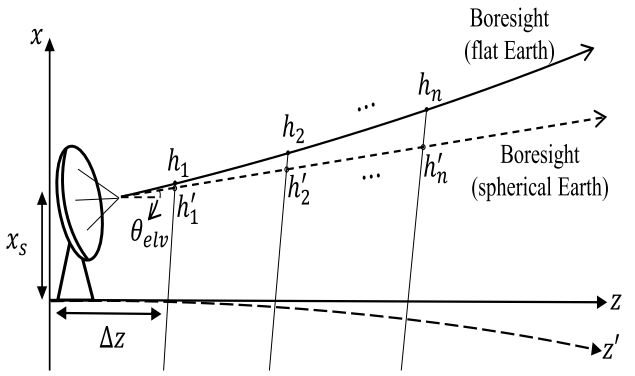

FIGURE 5. Antenna boresight in spherical and flat Earth models. The boresight height on a flat earth h_n is determined by the antenna height x_s and the range increment Δz, as well as the elevation angle θ_{elv}.

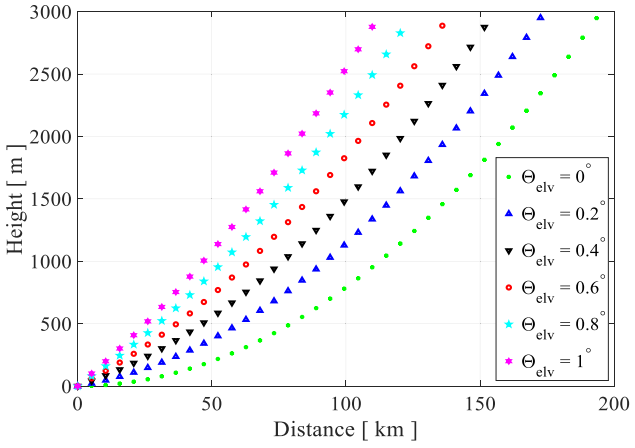

FIGURE 6. Compensated antenna boresight for elevation angles ranging from 0° to 1°.

where $sin\,(\theta\,(p)) = \lambda p$, and B is the normalized beam pattern function with a value of 1 at boresight. In the SSPE method, the initial value is crucial for accurate modeling of propagation. However, obtaining an actual antenna pattern can sometimes be difficult. In long–range propagation environments, the sharp main beam of an antenna has a significant impact, making simple modeling an effective alternative. A gaussian antenna pattern is a reliable substitute for accurately modeling the initial value. The gaussian antenna pattern can be defined in the vertical wavenumber domain as [27]

$$g(k_x) = exp\left[\frac{-k_x^2 ln2}{2k_0^2 sin^2\,(\theta_{bw}/2)}\right] \tag{13}$$

where θ_{bw} represents the 3 dB beamwidth, and k_x is the Fourier transform pair with the height x. The initial field profile can be obtained by performing the following calculation using the gaussian antenna pattern $g(k_x)$, the height of the antenna x_s, the Fresnel reflection coefficient Γ and then performing an inverse Fourier transform on the result.

$$u(0, k_x) = g(k_x)exp(-ik_x x_s) + \Gamma g^*(-k_x)exp(ik_x x_s) \tag{14}$$

Additionally, the elevation angle of the antenna θ_{elv} can be introduced using the Fourier shift theorem.

In practical applications, all analyses and models are conducted within the context of a spherical Earth. Thus, on a spherical Earth, antenna's boresight is typically aligned linearly. However, when utilizing the PE method, the analysis involves a transformation from the spherical Earth to a flat Earth. In this process, it becomes crucial to ensure accurate compensation for the boresight alignment. In this way, it is possible to accurately compare the analysis result of the refracted direction of antenna's main beam derived by the PE method and the boresight. The antenna boresight on flat Earth model is compensated as illustrated in Fig. 5.

To achieve it, the first step is to discretize the boresight into range increments Δz. The height of the boresight h_n is then calculated as it advances by the Δz, based on the previous boresight height h_{n-1}, the known height x_s and elevation angle θ_{elv} of the antenna. Finally, the compensated boresight height according to the Δz is obtained with the radius of Earth a_e as

$$h_n = \frac{cos(\theta_{elv})}{cos(\theta_{elv} + n\Delta z/a_e)}(a_e + x_s) - a_e \tag{15}$$

To investigate the effect of Earth flattening on the boresight, we utilized (15) to compute the boresight for an antenna at a height of 0 m and with varying elevation angles ranging from 0° to 1°. The obtained results are illustrated in Fig. 6. In the context of a spherical Earth, it becomes evident that the boresight, which ideally maintains a straight trajectory corresponding to the elevation angle, undergoes a compensatory adjustment, curving upwards in a flat Earth model.

B. PATH LOSS PROFILE AND REFRACTED DIRECTION OF MAIN BEAM

By incorporating both atmospheric and geographical modeling and utilizing the DMFT–SSPE method within the analysis area, the path loss profile for distance and height can be calculated. This result allows us to identify the refracted direction of antenna's main beam by analyzing the point with the lowest path loss for each distance. To verify the reliability of the analysis method, it is compared with the results from the Advanced Refractive Effects Prediction System (AREPS) using four different refraction models. AREPS is one of the computer software developed for military purposes [28]. The public version of AREPS utilizes a uniform refractivity throughout the entire analysis domain. To enable the comparison and analysis of the results obtained from both the proposed method and AREPS, the atmospheric condition is modeled using the same refractivity applied uniformly for all distances. For the PE analysis, the upper altitude limit is defined at 3000 m above sea level. An antenna is positioned at the midpoint of the analysis range (1500 m), and the elevation angle of the antenna is set as 0°. The results of the PE analysis and AREPS simulation are analyzed

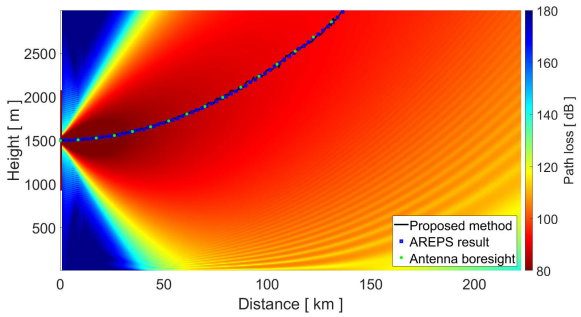

(a)

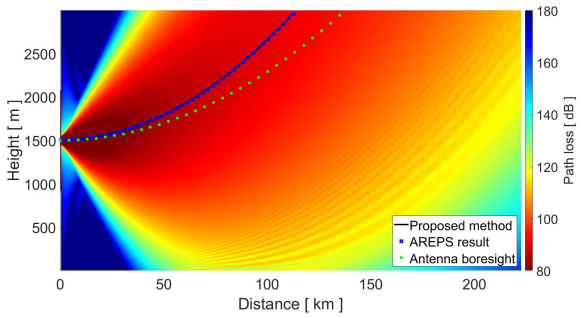

(b)

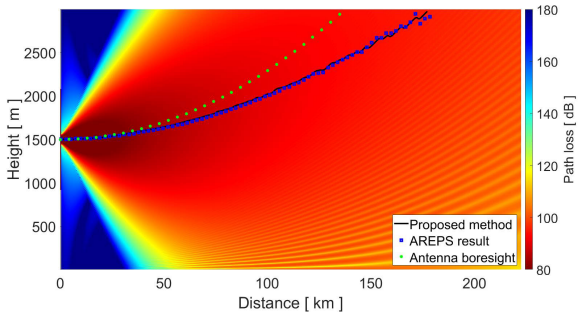

(c)

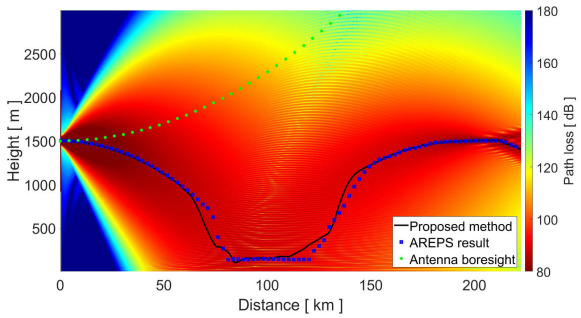

(d)

FIGURE 7. **Path loss profile analysis with four different atmospheric conditions. By comparing the refracted direction of main beam (black solid line) with the boresight (green dotted line), it is possible to verify the general trend of EM wave propagation. (a) Free space ($\nabla M = 157$). (b) Sub–refraction ($\nabla M = 230$). (c) Normal–refraction ($\nabla M = 100$). (d) Duct ($\nabla M = -300$).**

to illustrate the path of the refracted main beam, and it is compared with the boresight calculated with (15).

The atmosphere is considered as free space, assuming a refractive index of $n = 1$, which results in a vertical gradient ∇M of 157. Based on this, the entire domain is modeled as free space, and the path loss profile is analyzed and presented in Fig. 7a. EM waves theoretically propagate in free space without being refracted. The analysis result confirms that the direction of the antenna boresight, the path loss profile tendency (the reddest part), and the refracted main beam direction tend to coincide.

When the vertical gradient of refractive index, as determined by ∇M, exceeds 157, EM waves bend upwards from the antenna boresight, resulting in a sub–refraction state. To investigate the effects of sub–refraction, we set the ∇M of the entire domain to 230. The results of the analysis are presented in Fig. 7b, which shows an overall upward bias in the path loss trend compared to the antenna boresight. Additionally, the analysis of the refracted main beam direction confirms that the waves are deflected above the antenna boresight.

Normal–refraction occurs when ∇M ranges from 78 to 157, and super–refraction occurs when ∇M ranges from 0 to 78, resulting in EM waves being refracted below the antenna boresight. We investigated normal–refraction by modeling the atmosphere using the ∇M of 100. The results, shown in Fig. 7c, indicate a downward bias in the path loss trend compared to the antenna boresight. Analysis of the refracted main beam direction confirms that the waves are biased below the antenna boresight.

Occasionally, a phenomenon known as duct occurs, wherein EM waves propagate into non-line-of-sight (NLOS) areas at considerable distances. In such cases, ∇M for the region where the EM waves are trapped has a negative value. Although duct is not a common case, it often occurs in the case of EM wave propagation around the ocean. To investigate the effects of this phenomenon, we modeled the atmosphere using an ∇M of -300 and performed the analysis. The outcomes presented in Fig. 7d demonstrates that EM waves do not follow a straightforward path but tend to travel extended distances by reflecting and bouncing off the ground. The negative value of ∇M makes EM waves bend toward the ground, and the reflected waves also curve back down, showing trapping behavior. A same trend is observed in the refracted main beam direction.

Basically, all of the results about propagation path prediction are consistent with those obtained using AREPS. The results revealed that the theoretical tendency of EM wave propagation aligned with the refracted direction of main beam. Thus, this approach can predict the tendency of EM wave propagation in a given area and calculate the difference from the antenna boresight and the refracted direction of main beam.

In Fig. 8, we calculated the difference between the antenna boresight and the refracted main beam direction shown in Fig. 7. In free space, EM waves propagate along the antenna boresight, so there's no deviation as distance increases. However, in sub– and normal refraction, the differences are positive and negative, respectively. Sub refraction causes EM waves to propagate upward the antenna boresight,

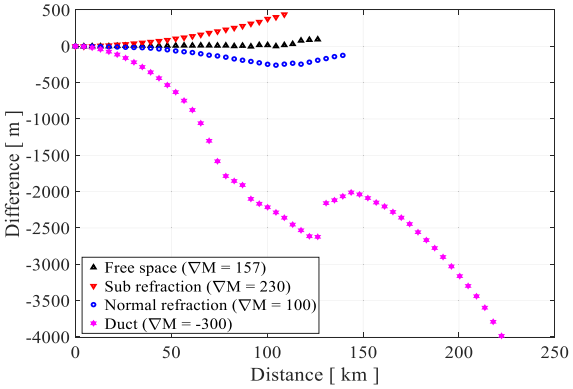

FIGURE 8. The differences between the refracted direction of main beam and the boresight under four atmospheric conditions.

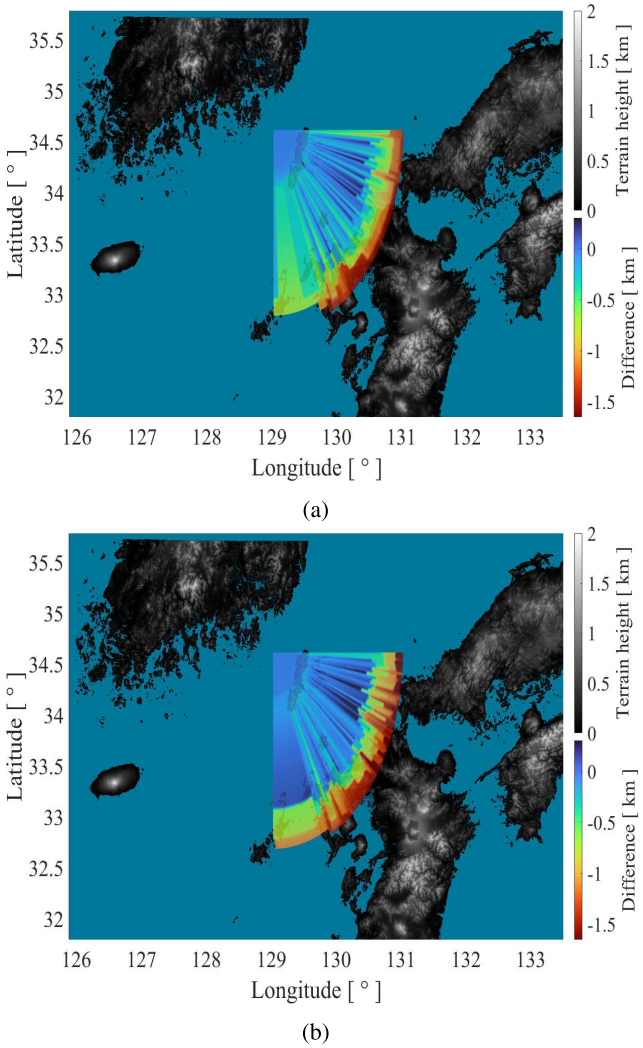

FIGURE 9. Difference map of the area 90° counterclockwise from the south of the radar position. (a) IDW interpolation. (b) kriging interpolation.

while normal refraction makes them travel downward. Furthermore, under duct atmospheric conditions, EM waves propagate long distances through repeated refraction and ground reflection, resulting in a negative difference across an extensive range.

Furthermore, the difference between refracted direction of main beam and boresight is calculated on the analysis area corresponding to 90° counterclockwise from the south of the radar position as illustrated in Fig. 9. The N generated through IDW and kriging interpolation, and terrain profile are applied. The N used in the analysis has the characteristics of sup–refraction. Thus, the results of applying both interpolation methods indicate that the refracted direction of main beam is formed in a downward compared to the boresight, and the value of difference is negative. Moreover, the results show fluctuations when the angle exceeds approximately 20° within the analysis area, which may be due to the effect of topography located directly in front of the radar position, causing distortions in the propagation of the EM wave. In conclusion, the results will make it possible to calculate the radar detection error.

IV. SLANT RANGE ERROR AND ANGULAR ERROR

Radar detection expresses the actual position of target as slant range and angle using radar echo time. The radar echo time means the time it takes for EM waves emitted from the radar antenna to return to the radar after being reflected by the target. Therefore, by tracing the propagation path for half of the radar echo time, the position of the target detected by the radar can be inferred. In general, the propagation path is traced relative to the antenna boresight. However, in reality, the propagation path may not coincide with the boresight, and the speed of the waves is affected by the N, leading to errors in target detection. This study aims to predict the radar detection error in long–range environment corresponding to slant range and angular error. For prediction, a comparison of the refraction path and the boresight is required. That is, after determining the position of the target for each path by applying the radar echo time, the error can be calculated by obtaining the difference between the two. The range of received echo time is set between 0.2 ms and 1 ms arbitrarily.

In real–world scenarios, the N of the atmosphere is different from that of free space, which slows down the propagation speed of EM waves. This difference can cause a distance difference of several tens to about a hundred meters within the range of the radar echo assumed in this study. In particular, when analyzing EM waves over long range, the slant range error may increases, making it essential to consider the propagation speed. To accomplish this, the propagation path need to be discretized and the distances between each point should be calculated. Then, the velocity of the EM wave along the path can be calculated using the refractive index n_i at the i–th point as

$$v_i = \frac{3 \times 10^8}{n_i} \tag{16}$$

Calculating the time it takes to travel through the propagation path allows us to determine the distance that an EM wave travels during half of the radar echo time. As a result,

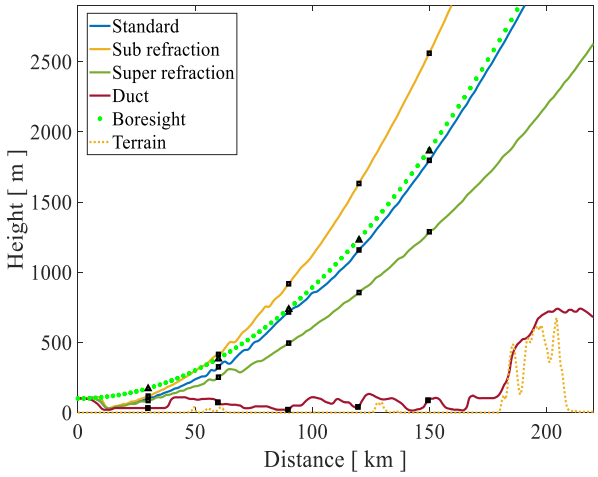

FIGURE 10. Arrival positions of EM waves at different radar echo time at 45° of the analysis area. The black triangular point represents the arrival point for each time when the EM wave travels at the speed of light on the boresight, while the black square point indicates a point on the refracted direction path at the speed of v_i.

it becomes possible to find the position where the EM wave arrives on the propagation path and the boresight with respect to the same radar echo time. Comparing these positions, the slant range and angular error can be calculated.

Assuming a case of oriented at 45° among the analysis areas in Fig. 3, the refracted main beam direction considering the terrain and atmospheric environment is analyzed and shown in Fig. 10. For each refraction case, all refracted direction are the same as the theory, and it is confirmed that some distortion occurred due to multipath effect due to the terrain. In addition, after each refracted path is discretized, (16) is applied to indicate the EM wave arrival position for a total of 5 radar echo times from 0.2 to 1 ms as black dots in Fig. 10.

It is confirmed that a slight distance difference occurs at the arrival position of the EM wave with the same radar echo time since each refracted path has different path length. Through this process, it is possible to obtain the arrival position of the EM wave in the boresight and refracted main beam direction path for an arbitrary radar echo time. Then, using the distance and altitude values of their position, the calculation of the slant range and angular error for the position of the target becomes possible.

Table 1 and 2 present the results of analyzing the slant range and angular error for different analysis domains (0°, 45°, and 90°) with atmospheric modeling using IDW and kriging. And, the errors of the target detection for the radar echoes of 0.3, 0.6, and 0.9 ms are calculated. A negative sign in the slant range and angular error indicates that the position of the actual target predicted on the refracted main beam direction path is analyzed to be closer and lower than the position determined by the radar on the boresight path respectively. The analysis shows that most

TABLE 1. Radar error calculation result using IDW.

Analysis angle \ Echo time [ms]		0.3	0.6	0.9
0°	Slant range error [m]	-13.97	-29.87	-49.42
	Angular error [°]	-0.06	-0.17	-0.06
45°	Slant range error [m]	-13.99	-31.36	-50.42
	Angular error [°]	-0.04	-0.01	-0.06
90°	Slant range error [m]	-13.98	-38.27	-56.82
	Angular error [°]	-0.05	-0.23	-0.18

TABLE 2. Radar error calculation result using kriging.

Analysis angle \ Echo time [ms]		0.3	0.6	0.9
0°	Slant range error [m]	-14	-31.5	-52.45
	Angular error [°]	0	-0.01	0.05
45°	Slant range error [m]	-14	-31.24	-50.88
	Angular error [°]	0	-0.14	-0.08
90°	Slant range error [m]	-14	-31.8	-51.38
	Angular error [°]	-0.03	-0.12	-0.08

of the predicted values are located in the lower direction than the boresight, suggesting the presence of a normal– or super–refractive atmosphere. However, occasionally a positive value on angular error is derived, indicating that the refracted main beam direction is formed above the boresight due to multipath effect by the terrain. The radar detection error is calculated using the atmospheric model applied with two conventional interpolation methods, IDW and kriging, but it is confirmed that no significant difference occurred.

Through this process, the radar detection error for the entire analysis area in Fig. 3 is analyzed as illustrated in Fig. 11. A shorter echo time implies detecting a target from a closer location. When EM waves propagate over a very short distance, the error is close to 0. However, as echo time increases, interaction with various environments causes deviations between antenna boresight and refracted main beam direction, resulting in radar detection error. Results obtained using both IDW and kriging methods indicate a similar trend in slant range error, and the angular error consistently follows this trend, except for a noticeable difference ranging from 0° to about 30°. This arises from variations in the refractivity interpolation outcomes shown in Fig. 4. As suggested in this paper, by dividing the errors into slant range and angular error, and analyzing it as a map over the entire analysis area, the radar detection error can be corrected by checking the value of the error by target location, that is, by radar echo time.

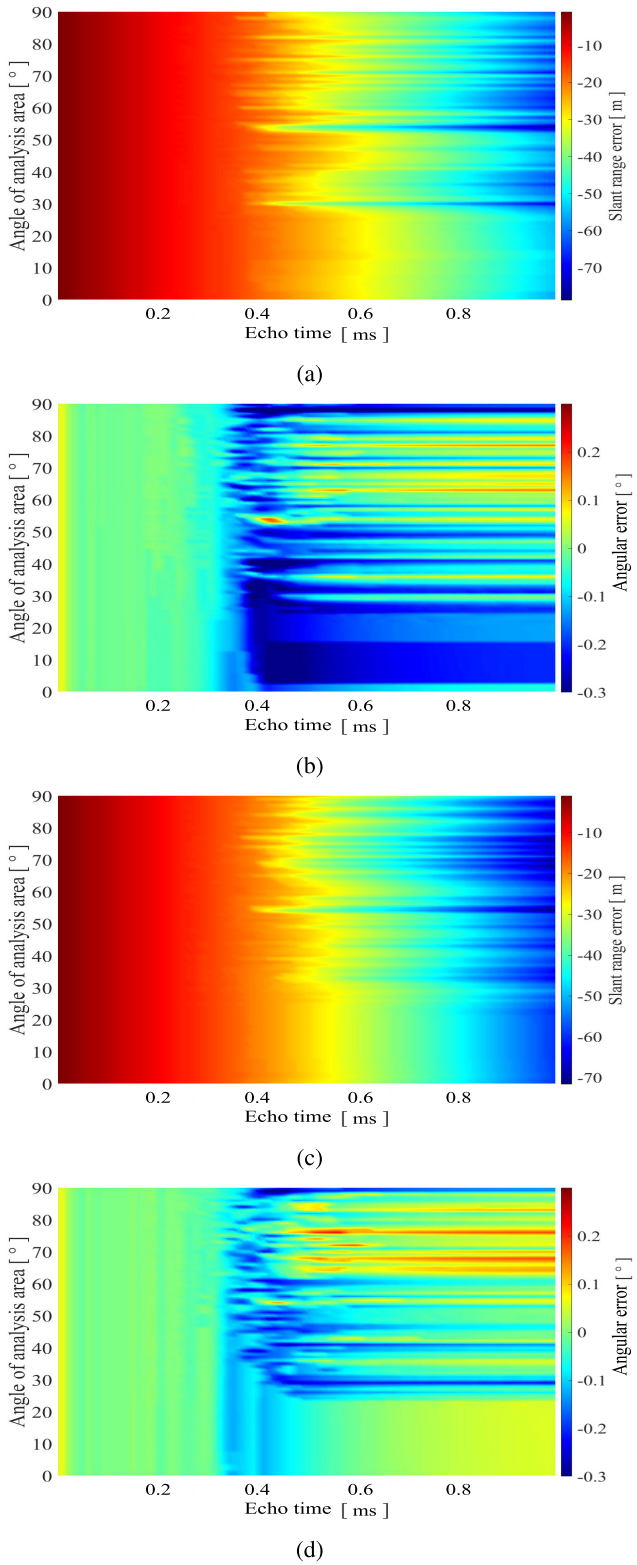

FIGURE 11. Radar errors for the entire analysis area. (a) Slant range error (IDW). (b) Angular error (IDW). (c) Slant range error (kriging). (d) Angular error (kriging).

V. CONCLUSION

We proposed a novel method to predict radar detection errors in long–range environment by considering slant range and angular error. Various ray tracing tools can be used to analyze the electromagnetic (EM) wave propagation, but they are inadequate to consider the effects of various long range environments. In particular, the refractivity that changes with distance has a significant impact on the propagation analysis, and a numerical analysis method that can take this into account was needed. Therefore, we conducted our analysis using discrete mixed Fourier transform based split–step parabolic equation method, which can take into account environmental impacts that change with distance. The two-dimensional refractivity within the analysis area was modeled using meteorological data collected on a specific day. The direction of refracted antenna's main beam was predicted using the path loss, and by comparing it with the antenna boresight, the radar detection errors were computed according to the received time of the radar echo. Through the proposed analysis, it was possible to predict how the propagation path of the EM wave is refracted in a certain range from the radar position, and how much the EM wave travels for a fixed time through that path. By comparing the position along the refracted path with the position along the boresight, it becomes possible to estimate radar detection errors for analysis area. In general, radar systems determine a target's location assuming free space conditions, where EM waves propagate exactly as the antenna boresight. Therefore, our proposed method for calculating a target's position by predicting the refracted main beam direction, accounting for long–range environmental effects like refraction, offers a means to enhance radar detection accuracy. The error determined using the proposed method can be added to the target's location calculated in free space to estimate the actual target location.

REFERENCES

[1] K. A. Norton, "The propagation of radio waves over the surface of the earth and in the upper atmosphere," *Proc. IRE*, vol. 24, no. 10, pp. 1367–1387, Oct. 1936.

[2] J. R. Wait, *Electromagnetic Waves in Stratified Media: Revised Edition Including Supplemented Material*, vol. 3. Amsterdam, The Netherlands: Elsevier, 2013.

[3] G. Millington, "Ground-wave propagation over an inhomogeneous smooth earth," *Proc. IEE III, Radio Commun. Eng.*, vol. 96, no. 39, pp. 53–64, Jan. 1949.

[4] G. Millington and G. A. Isted, "Ground-wave propagation over an inhomogeneous smooth earth. Part 2: Experimental evidence and practical implications," *Proc. IEE III, Radio Commun. Eng.*, vol. 97, no. 48, pp. 209–221, Jul. 1950.

[5] M. Levy, *Parabolic Equation Methods for Electromagnetic Wave Propagation*, document IET 45, 2000.

[6] L. Sevgi, "A ray-shooting visualization MATLAB package for 2D ground-wave propagation simulations," *IEEE Antennas Propag. Mag.*, vol. 46, no. 4, pp. 140–145, Aug. 2004.

[7] M. Leontovich and V. Fock, "Solution of the problem of propagation of electromagnetic waves along the earth's surface by the method of parabolic equation," *J. Phys. USSR*, vol. 10, no. 1, pp. 13–23, 1946.

[8] R. H. Hardin and F. D. Tappert, "Application of the split-step Fourier method to the numerical solution of nonlinear and variable coefficient wave equations," *SIAM Rev.*, vol. 15, p. 423, Jan. 1973.

[9] G. D. Dockery and G. C. Konstanzer, "Recent advances in prediction of tropospheric propagation using the parabolic equation," *Johns Hopkins APL Tech. Dig.*, vol. 8, pp. 404–412, Dec. 1987.

[10] G. D. Dockery, "Modeling electromagnetic wave propagation in the troposphere using the parabolic equation," *IEEE Trans. Antennas Propag.*, vol. AP-36, no. 10, pp. 1464–1470, Mar. 1988.
[11] K. H. Craig, "Propagation modelling in the troposphere: Parabolic equation method," *Electron. Lett.*, vol. 24, no. 18, pp. 1136–1139, Sep. 1988.
[12] A. E. Barrios, "Parabolic equation modeling in horizontally inhomogeneous environments," *IEEE Trans. Antennas Propag.*, vol. 40, no. 7, pp. 791–797, Jul. 1992.
[13] L. Sevgi, "A mixed-path groundwave field-strength prediction virtual tool for digital radio broadcast systems in medium and short wave bands," *IEEE Antennas Propag. Mag.*, vol. 48, no. 4, pp. 19–27, Aug. 2006.
[14] L. Sevgi, C. Uluisik, and F. Akleman, "A MATLAB-based two-dimensional parabolic equation radiowave propagation package," *IEEE Antennas Propag. Mag.*, vol. 47, no. 4, pp. 164–175, Aug. 2005.
[15] J. R. Kuttler and G. D. Dockery, "Theoretical description of the parabolic approximation/Fourier split-step method of representing electromagnetic propagation in the troposphere," *Radio Sci.*, vol. 26, no. 2, pp. 381–393, Mar. 1991.
[16] J. R. Kuttler and R. Janaswamy, "Improved Fourier transform methods for solving the parabolic wave equation," *Radio Sci.*, vol. 37, no. 2, pp. 1–11, Apr. 2002.
[17] D. J. Donohue and J. R. Kuttler, "Propagation modeling over terrain using the parabolic wave equation," *IEEE Trans. Antennas Propag.*, vol. 48, no. 2, pp. 260–277, Jul. 2000.
[18] G. Apaydin and L. Sevgi, "A novel split-step parabolic-equation package for surface-wave propagation prediction along multiple mixed irregular-terrain paths," *IEEE Antennas Propag. Mag.*, vol. 52, no. 4, pp. 90–97, Aug. 2010.
[19] S. Choi, J. Heo, C. Kim, S. Wang, H. Choo, and Y. B. Park, "Prediction of electromagnetic wave propagation in troposphere using parabolic equation and two-dimensional refractivity," *J. Electr. Eng. Technol.*, vol. 15, no. 3, pp. 1287–1292, May 2020.
[20] X. Deng, C. Liao, D. Zhang, J. Feng, Y. Shang, and H. Zhou, "A novel PE/FDTD hybrid model for predicting echo signals of radar targets in large-scale complex environments," *IEEE Access*, vol. 8, pp. 28450–28461, 2020.
[21] V. A. Permyakov, M. S. Mikhailov, and E. S. Malevich, "Analysis of propagation of electromagnetic waves in difficult conditions by the parabolic equation method," *IEEE Trans. Antennas Propag.*, vol. 67, no. 4, pp. 2167–2175, Apr. 2019.
[22] S. Wang, T. H. Lim, and H. Choo, "Path loss analysis considering atmospheric refractivity and precipitation for air-to-ground radar," *IEEE Antennas Wireless Propag. Lett.*, vol. 20, no. 10, pp. 1968–1972, Oct. 2021.
[23] C. A. Balanis, *Advanced Engineering Electromagnetics*. Hoboken, NJ, USA: Wiley, 2012.
[24] *The Radio Refractive Index: Its Formula and Refractivity Data*, document ITU-R P. 453-14, 2019.
[25] S. Bhattacharjee, P. Mitra, and S. K. Ghosh, "Spatial interpolation to predict missing attributes in GIS using semantic kriging," *IEEE Trans. Geosci. Remote Sens.*, vol. 52, no. 8, pp. 4771–4780, Aug. 2014.
[26] C. Liu, A. Kiring, N. Salman, L. Mihaylova, and I. Esnaola, "A Kriging algorithm for location fingerprinting based on received signal strength," in *Proc. Sensor Data Fusion, Trends, Solutions, Appl. (SDF)*, 2015, pp. 1–6.
[27] G. Apaydin and L. Sevgi, *Radio Wave Propagation and Parabolic Equation Modeling*. Hoboken, NJ, USA: Wiley, 2017.
[28] W. L. Patterson, "Advanced refractive effects prediction system (AREPS)," in *Proc. IEEE Radar Conf.*, Apr. 2007, pp. 891–895.

JUN HEO (Graduate Student Member, IEEE) received the B.S. degree in electrical and computer engineering from Ajou University, Suwon, South Korea, in 2018, where he is currently pursuing the integrated M.S. and Ph.D. degrees in AI convergence networks. His research interests include electromagnetic wave propagation, radar performance analysis, and wireless power transmission.

JUNMO YANG (Graduate Student Member, IEEE) received the B.S. degree in electrical and computer engineering from Ajou University, Suwon, South Korea, in 2021, where he is currently pursuing the integrated M.S. and Ph.D. degrees in AI convergence networks. His research interests include electromagnetic wave propagation and machine learning.

JONGMANN KIM received the B.S. degree in electronic and electrical engineering from Kyungpook National University, Daegu, South Korea, in 2002, the M.S. degree in electronic and electrical engineering from the Pohang University of Science and Technology (POSTECH), Pohang, South Korea, in 2004, and the Ph.D. degree in electrical and electronic engineering from Yonsei University, Seoul, South Korea, in 2021. Since 2005, he has been with the Agency for Defense Development (ADD), Daejeon, South Korea. His current research interests include radar signal and data processing.

DONG-YEOP NA (Member, IEEE) received the B.S. and M.S. degrees in electrical and computer engineering from Ajou University, Suwon, South Korea, in 2012 and 2014, respectively, and the Ph.D. degree in electrical and computer engineering from The Ohio State University, Columbus, OH, USA, in 2018. From 2019 to 2022, he was with the Elmore Family School of Electrical and Computer Engineering, Purdue University, West Lafayette, IN, USA, as a Postdoctoral Research Associate and Research Scientist. He joined the Department of Electrical Engineering, Pohang University of Science and Technology, Pohang, South Korea, in 2022, where he is currently an Assistant Professor. His research interests include computational electromagnetics, kinetic plasma modeling via particle-in-cell algorithm, and quantum electromagnetics.

YONG BAE PARK (Senior Member, IEEE) received the B.S., M.S., and Ph.D. degrees in electrical engineering from the Korea Advanced Institute of Science and Technology, South Korea, in 1998, 2000, and 2003, respectively. From 2003 to 2006, he was with the Korea Telecom Laboratory, Seoul, South Korea. He joined the School of Electrical and Computer Engineering, Ajou University, South Korea, in 2006, where he is currently a Professor. His research interests include electromagnetic field analysis, high-frequency methods, metamaterial antennas, radomes, and stealth technology.